Published October 1, 1996

Dilation of the Influenza Hemagglutinin Fusion Pore Revealed by the Kinetics of Individual Cell–Cell Fusion Events

Robert Blumenthal,* Debi P. Sarkar,§ Stewart Durell,‡ Daniel E. Howard,‖ and Stephen J. Morris‖

*Section on Membrane Structure and Function, and ‡Molecular Structure Section, Division of Basic Sciences, National Cancer Institute, National Institutes of Health, Bethesda, Maryland 20892; §Department of Biochemistry, University of Delhi South Campus, New Delhi, India; and ‖Division of Molecular Biology and Biochemistry, School of Biological Sciences, University of Missouri-Kansas City, Kansas City, Missouri 64110-2499

Abstract. We have monitored kinetics of fusion between cell pairs consisting of a single influenza hemagglutinin (HA)–expressing cell and a single erythrocyte (RBC) that had been labeled with both a fluorescent lipid (DiI) in the membrane and a fluorescent solute (calcein) in the aqueous space. Initial fusion pore opening between the RBC and HA-expressing cell produced a change in RBC membrane potential ($\Delta\psi$) that was monitored by a decrease in DiI fluorescence. This event was followed by two distinct stages of fusion pore dilation: the flux of fluorescent lipid (ϕ_L) and the flux of a large aqueous fluorescent dye (ϕ_S). We have analyzed the kinetics of events that occur as a result of transitions between a fusion pore (FP) and a solute permissive fusion pore (FP_S). Our data are consistent with a fusion pore comprising six HA trimers.

FUSION of the influenza virus membrane with that of the host cell is mediated by hemagglutinin (HA)[1] (47) and triggered by the low pH environment within the endosome (46). To dissect the events that occur after the low pH triggering of HA, we have performed kinetic studies of fusion of fluorescently labeled virus and cells. One of the interesting characteristics of the kinetics is the appearance of delays in lipid redistribution after low pH triggering, suggesting a multistep process (2). The mechanism of cell fusion mediated by HA was further investigated by monitoring fusion of single erythrocytes (RBCs), stained with fluorescent lipids and solutes, with cells expressing HA (19, 31, 38). By using simultaneous measurements of pairs of assays for fusion, the order of detectable events during fusion was determined (45, 49). Fusion pore formation in HA-triggered cell–cell fusion was first detected by changes in cell membrane capacitance (24, 25, 42, 43, 45, 49), next by a flux of fluorescent lipid (26, 45, 49), and finally by a flux of aqueous fluorescent dye (49). This sequence of events was revealed by a combination of electrical admittance and quantitative fluorescence video microscopy techniques.

To study kinetics of fusion pore dilation, it is necessary to collect a large data set on single cell–cell fusion events. This was not possible using the capacitance patch clamp technique with HA-expressing cells. However, Tse et al. (45) observed that the initial capacitance change associated with the formation of a fusion pore between the RBC and HA-expressing cell occurred concomitantly with a change in the fluorescence intensity of DiI in the RBC membrane. The decrease in DiI fluorescence is presumably due to a change in RBC membrane potential ($\Delta\psi$), which occurs when the RBC inner space becomes continuous with that of the HA-expressing cell. This $\Delta\psi$ event occurs simultaneously with the capacitance change, when measured on a time scale of seconds. Using a specially constructed fluorescence video microscope that allows for simultaneous, real-time, video rate imaging of up to four fluorophores (30,33), our laboratories have been studying the sequence of events involved in HA-induced cell–cell fusion. We have examined these sudden decreases in DiI fluorescence, which precede lipid flow. These experiments demonstrate that the imaging system is fully capable of resolving $\Delta\psi$ with at least the time resolution of cell–cell fusion by electrical admittance measurements (34). The multi-wavelength imaging system enabled us to collect sufficient data to perform a kinetic analysis of the transition from fusion pore (FP) to FP_S.

Materials and Methods

Cell Lines

GP4F cells (mouse 3T3 fibroblasts stably expressing wild-type HA) (12, 31) and glycosylphosphatidylinositol (GPI)–HA-expressing CHO cells

Address all correspondence to Robert Blumenthal, Section on Membrane Structure and Function, National Institutes of Health, 10 Center Drive, MSC 1350, Building 10/Room 4A01, Bethesda, MD 20892-1350. Tel.: (301) 496-8832. Fax: (301) 402-3650. e-mail: blumen@helix.nih.gov.

1. *Abbreviations used in this paper*: BSS, balanced salt solution; FP, fusion pore; GPI, glycosylphosphatidylinositol; HA, hemagglutinin; ROI, region of interest.

Published October 1, 1996

were grown in tissue-culture flasks in DME containing 5% FBS at 37°C, 10% CO_2 as described (20, 26, 32). The GPI–HA-expressing cells were maintained in glutamine-deficient DME containing 400 μM methyl sulfoxamine to maintain selection. Those cells were split for fusion experiments by lifting in cell dissociation buffer and replated in glutamine-deficient DME containing 400 μM methyl sulfoxamine and 250 μM deoxymannojirimycin to block terminal mannosylation. Best results were obtained when cells were used after 48–72 h after replating.

Preparation of Double-labeled Human Erythrocyte Ghosts

Human RBCs were freshly isolated from whole blood and suspended at 50% hematocrit in balanced salt solution (BSS): 138 mM NaCl, 4 mM KCl, 2 mM $CaCl_2$, 2 mM $MgCl_2$, 20 mM Hepes, pH 7.30. 10 ml of 1% hematocrit RBC in BSS at room temperature was rapidly mixed with 25 μl of 1 mg/ml DiI(C18-3) (Molecular Probes, Inc., Eugene, OR) in ethanol and washed. These RBCs were converted into ghosts and resealed in the presence of 3 mM calcein, 130 mM KCl, 10 mM Hepes, pH 7.05, using the method described by Clague et al. (9).

Decoration of HA-expressing Cells with Double-labeled RBC

It was important for the video imaging and subsequent analysis of cell–RBC fusion to produce cells to which only a single RBC was bound. The HA and GPI–HA-expressing cells were decorated in the flasks with double-labeled RBC ghosts using the following protocol (32): after rinsing the flask twice with PBS, the HA was activated by treatment with 2 ml trypsin (5 μg/ml) and neuraminidase (220 μg/ml) for 5 min in Hepes-buffered BSS. After the addition of 1 mg/ml soybean trypsin inhibitor in BSS or complete DME containing 10% FBS to block trypsin activity, the flasks were washed twice with DME (no serum), and 5 ml of DME was added. The fibroblasts were decorated with the double-labeled RBC by adding 50–100 μl of 0.1% hematocrit suspension of RBC to the flask and by allowing the RBC to settle onto the cells for 10 min or until the majority of cells had only one RBC bound. Unbound RBCs were removed by two gentle BSS washes. The decorated cells were then lifted with 0.5 mg/ml trypsin and 0.2 mg/ml EDTA in BSS. The trypsin was again blocked with complete medium plus serum or soybean trypsin inhibitor, centrifuged, resuspended in BSS, and held at 0–4°C until use.

Fluorescence Recording Procedures

A polylysine-coated 10 × 10 mm glass coverslip (#00; Corning, Inc., Corning, NY) was placed in 1.0 ml of BSS in a thermostatted environment chamber with a thin (#0) glass bottom, of the type used for patch clamp studies. 10–20 μl of a suspension of labeled cell–RBC complexes were gently pipetted onto the coverslip, and the cells were illuminated, as described above, and imaged with a ×100 phase fluor DL oil immersion, 1.30 NA objective (Nikon Inc., Garden City, NY). The examination of the fusion of the cell–RBC ghost complexes by multi-wavelength fluorescence video microscopy was accomplished as described (34). The video recordings were subjected to a series of off-line analyses. First, to establish the basic changes in fluorescence from the addition of the low pH buffer to after the beginning of soluble dye movement (usually >5 min), four regions of interest (ROIs) were drawn as follows (see Fig. 1).: (1) an outline of the green fluorescence from calcein seen in the RBC, (2) a roughly circular ROI, well inside the periphery of the calcein fluorescence in the GP4F cell, as judged from the final fluorescence and phase-contrast images, (3) a similar outline of the red fluorescence from DiI seen in the RBC, and (4) an irregular ROI on the DiI fluorescence image of the GP4F cell, drawn to just exclude the RBC but include the areas of the GP4F plasma membrane where the DiI would begin to spread. The tape was then played back to the digital video analysis system. The integrated gray levels of 25 consecutive frames for the four ROIs were averaged and saved. The resulting data were then plotted using SigmaPlot 5.0 software (Jandel Scientific, San Rafael, CA) (see Fig. 2). This graph was used to establish the time between the lowering of the pH and the start of lipid redistribution, and the elapsed time from the beginning of the membrane probe movement to movement of the soluble probe ($\Delta\phi_L \rightarrow \Delta\phi_S$). The graphs were also used to search for those fusion events where a decrease in membrane potential could be detected by a sudden sharp change in RBC DiI fluorescence occurring before the beginning of DiI redistribution (34), and to time the interval between this event and the establishment of lipid flow ($\Delta\psi \rightarrow \Delta\phi_L$) (see Fig. 2). The onset of lipid and solute flow was determined by eye. Determinations of lag times performed by three different investigators were within 2 s. Algorithms to obtain unbiased determinations of the lag times did not yield better results than "eye-balling." However, since we were concerned about a possible bias in the estimation of lag times, we used a random number generator to either add 2 s to or subtract 2 s from the lag times for the onset of solute permeation. The resulting data yielded an identical curve to that shown in Fig. 4.

Results

Detection of Single Cell Fusion Events

To obtain detailed information on the time course of the fusion of individual pairs of cells, we measured fluorescence changes in lipid and aqueous dyes using quantitative fluorescence video microscopy. Exposing the GP4F–RBC complex to pH 5 caused spreading of the dye over the surface of the GP4F cell and concomitant depletion of dye in the RBC membrane (19, 38, 49). Fig. 1 shows a montage of video images from a typical fusion experiment. A single GP4F fibroblast to which one double-labeled RBC has bound can be seen in the phase-contrast images in the top row. The fluorescence from the soluble calcein dye (λ_{em} = 530 nm) trapped within the double-labeled RBC and the membrane-bound DiI fluorophore (λ_{em} = 590 nm) was taken before and after the pH was changed to ~5.0. The images show the onset of membrane dye redistribution before the onset of soluble contents mixing (Fig. 1 *B*, *E*, and *H*) followed by redistribution of both DiI and calcein (Fig. 1 *C*, *F*, and *I*). The fluorescence changes were quantified by integrating pixel intensities over the indicated ROIs.

The integrated fluorescence from the fibroblast calcein and DiI and from RBC DiI is graphed in Fig. 2. The pH was changed to 5 at time 0. The DiI fluorescence in the RBC shows a distinct sharp drop ~20 s after the pH change. This sudden reduction in RBC DiI fluorescence, which precedes fusion-induced dye redistribution, has been attributed to a membrane potential change ($\Delta\psi$) leading to a flow of ions as a result of HA-induced pore formation (45). The increase in RBC DiI fluorescence ~50 s later is due to dequenching of the DiI, which has been incorporated at self-quenching concentrations. This eventually reverses as the DiI flows out of the RBC membrane into the fibroblast plasma membrane. DiI fluorescence in the fibroblast begins to increase ($\Delta\phi_L$) ~40 s after $\Delta\psi$. This is followed by a redistribution of the soluble calcein ($\Delta\phi_S$) ~100 s later. Thus, the sequence of events after the low pH triggering shown previously is preserved in these experiments.

Experiments with GPI-anchored HA-expressing Cells

Although Tse et al. (45) had shown that the decrease in DiI fluorescence informs us about fusion pore opening, we were concerned about possible artefacts. A perfect control for these experiments was provided by GPI–HA-expressing cells that under fusogenic conditions mediate redistribution of fluorescent lipid from RBC membranes to those cells without transfer of aqueous dye (20). By simultaneous video fluorescence microscopy and time-resolved electrical admittance measurements, Melikyan et al. (26) rigorously demonstrated that low pH interactions of GPI–HA-expressing cells with planar bilayer membranes re-

Published October 1, 1996

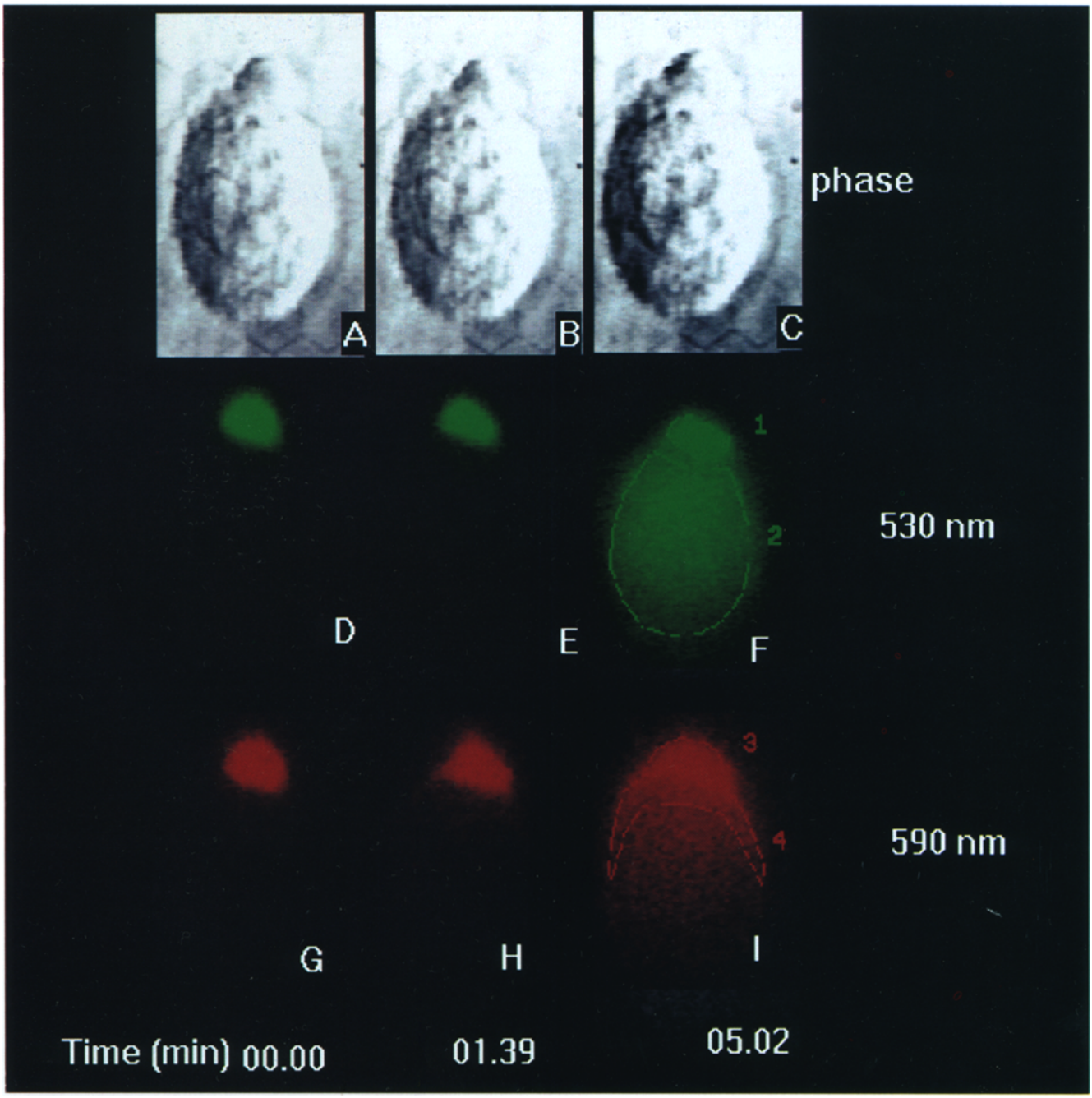

Figure 1. Video images of hemagglutinin-catalyzed GP4f/RBC fusion. 16 frame averages of various times before and during fusion of a calcein/DiI double-labeled RBC to a GP4f fibroblast as described in Materials and Methods. The video microscope set up to simultaneously acquire the two fluorescence and the phase-contrast images has been described in detail previously (30, 33, 34). (*A–C*) Phase-contrast images at 460 nm (*top row*). (*D–F*) Fluorescence emission of calcein at λ_{em} = 530 nm (*middle row*). (*G–I*) Fluorescence emission of DiI at λ_{em} = 590 nm (*bottom row*). (*A*, *D*, and *G*) Images taken at the time of the pH change (*right column*). (*B*, *E*, and *H*) Images taken ~1 min 39 s after the pH was lowered to 5, when DiI but not calcein starts moving into the fibroblast (*middle column*). (*C*, *F*, and *I*) Images taken at 5 min 2 s after the pH was lowered to 5, when the soluble dye has filled the cytoplasm of the fibroblast while the membrane-bound dye is spreading over the surface of the plasma membrane (*left column*). In Fig. 1 *F*, ROIs are drawn to define calcein fluorescence in the RBC (*1*) and the fibroblast (*2*), and in Fig. 1 *I*, ROIs are drawn to define DiI fluorescence in the RBC (*3*) and the fibroblast (*4*).

sulted in lipid continuity without formation of fusion pores. We confirmed the previous observations that membrane dye redistribution could be seen to proceed for >10 min with no movement of soluble dye. Table I shows that although a low pH -triggered decrease in DiI fluorescence was seen with wild-type HA-expressing cells in 60% of the cases, we observe no such decrease in GPI–HA-expressing cells. This indicates that the lipid redistribution mediated by GPI–HA is not preceded by the opening of a fusion pore. A decrease in DiI fluorescence is not always seen in

Published October 1, 1996

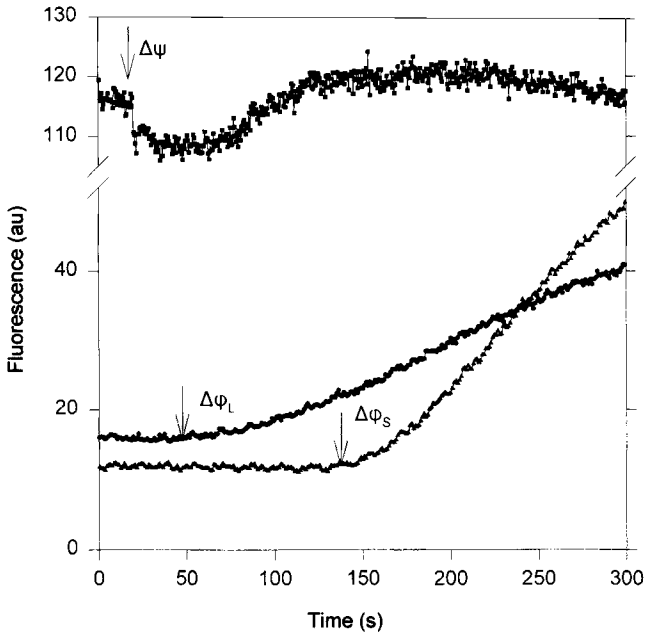

Figure 2. Dye redistribution kinetics. The average gray levels in three ROIs detailed in Fig. 1 were measured as a function of time after the pH was lowered to 5 (■): fluorescence in ROI 3 (see Fig. 1 *I*). The Δψ event (*arrow*) is seen as a sudden drop in the DiI fluorescence of the RBC. (●): fluorescence in ROI 4 (see Fig. 1 *I*). The start point of the lipid mixing $\Delta\phi_L$ (*arrow*) is clearly seen as a rise in fluorescence in the fibroblast membrane just adjacent to the RBC attachment site. ▲, fluorescence in ROI 2 (see Fig. 1 *F*). The start point of the soluble cytoplasmic dye redistribution ($\Delta\phi_S$; *arrow*) is seen as a rise in fluorescence in the fibroblast cytoplasm.

cases where lipid redistribution mediated by wild-type HA is observed (Table I). Possible explanations for this observation include already depolarized fibroblasts, or a RBC leaky enough not to be able to support a membrane potential after continuity with the fibroblast.

Kinetics of Fusion Pore Expansion

The total number of ΔpH → Δψ, ΔpH → $\Delta\phi_L$, and ΔpH → $\Delta\phi_S$ events that occurred within a given lag time are plotted in Fig. 3 as a function of time. The single channel-type kinetics clearly shows that fusion pore opening precedes lipid flow, and that lipid flow precedes solute flow. Although cumulative sums of lag times from ΔpH to initial fusion events have been presented previously (19, 24, 42),

Table I. Δψ Events Mediated by WT–HA and GPI–HA

Influenza hemagglutinin	Number of Δψ observations/total*	Percentage
		%
WT–HA‡	46/76	60
GPI–HA§	0/32	0

*Total number of DiI redistributions.
‡GP4F/RBC.
§GPI–HA-expressing CHO cells.

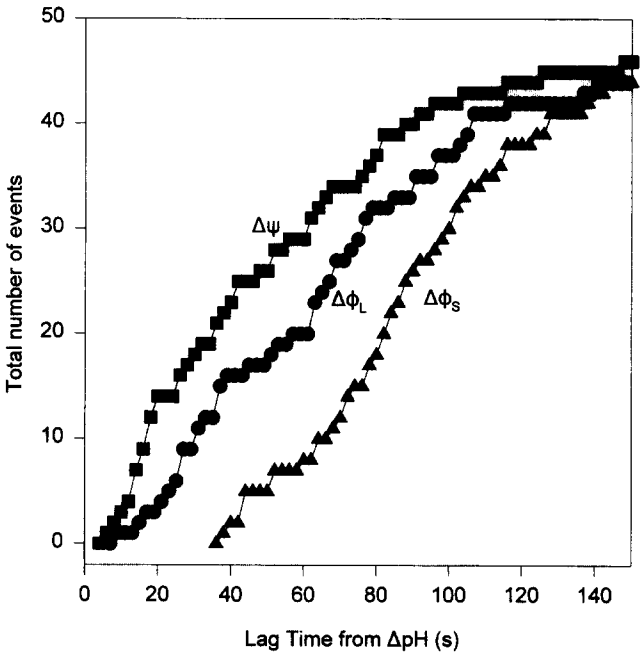

Figure 3. Kinetics of single fusion events. Summated curves from histograms show how many events occurred within a given time interval after lowering the pH to 5. ■, ΔpH → Δψ; ●, ΔpH → $\Delta\phi_L$; ▲, ΔpH → $\Delta\phi_S$.

the measurements in this study allow us to monitor kinetics of transition between two states: from FP to solute-permissive FP (FP_S). Fig. 4 shows the kinetics of the FP to FP_S transition, which follows an S-shaped time course very well characterized by Eq. 3 (see Discussion). To eliminate a possible bias in our determination of $\Delta\phi_S$, we used a random number generator to either add 2 s to or subtract 2 s from the lag times for the onset of solute permeation. The resulting data yielded an identical curve to that shown in Fig. 4.

Temperature Dependence

Fig. 5 shows the average time lags for the ΔpH → $\Delta\phi_L$ and the $\Delta\phi_L$ → $\Delta\phi_S$ transitions as a function of temperature. At temperatures below 37°C, we did not observe sufficient Δψ events to assess the Δψ → $\Delta\phi_L$ transition, nor did we collect a sufficient amount of data to perform the kinetic analysis. The temperature dependence of the ΔpH → $\Delta\phi_L$ cascade was steeper than that for the $\Delta\phi_L$ → $\Delta\phi_S$ transition.

Discussion

The Fusion Pore Formed by HA

An important new intermediate in HA-mediated fusion, the fusion pore, was revealed in single cell fusion studies by the differential dispersion of lipid, small aqueous molecules, and large molecules (38), and by electrical admittance studies (24, 25, 42, 43, 45, 49). Fusion pores have been previously identified in exocytosis (5, 6, 13, 27, 28,

Published October 1, 1996

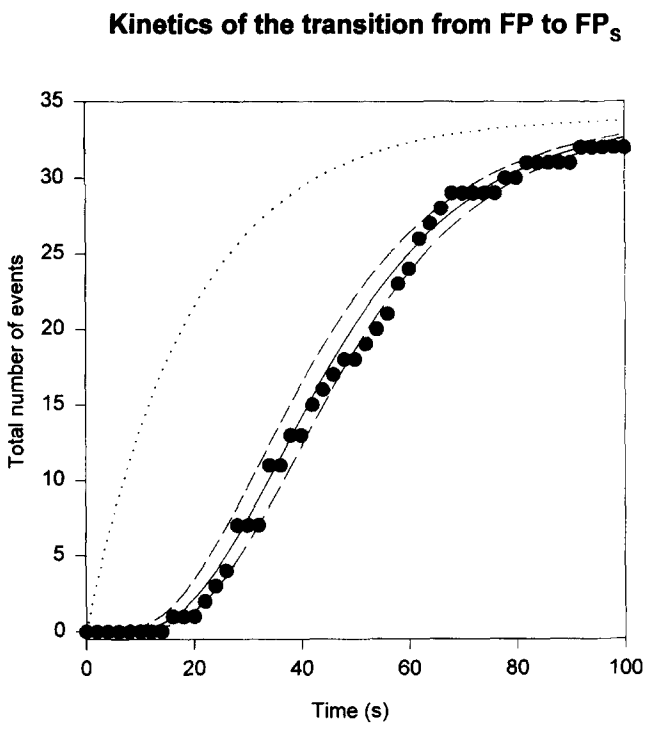

Figure 4. Kinetics of the transition from FP to FP_S. Summated curves from histograms of $\Delta\psi \rightarrow \Delta\phi_S$ transitions (●) were fit to $y = y\infty\ (1 - \exp(-k^*t)^n$. The fit yielded $n = 6.3$ and $k = 0.049$/s. The solid line is drawn with $n = 6$, the short-dashed line with $n = 5$, the long-dashed line with $n = 7$, and the stippled line with $n = 1$.

48) and are designed to make connections in highly localized areas.

In patch clamp experiments on HA-expressing fibroblasts fusing to erythrocytes, Spruce et al. (42) noted an increase in the fibroblast's membrane capacitance, indicating the opening of the fusion pore, the first aqueous connection between the fusing cells. These authors then showed that the capacitance increase is preceded by a brief current transient, generated as the erythrocyte discharges its membrane potential through the nascent fusion pore (43). From this signal, they deduced an initial pore conductance of 150 pS during the first milliseconds of its existence. The pore then grows more gradually over the subsequent tens of milliseconds until growth is arrested (25, 43, 49). This pore is initially an unstable structure frequently "flickering" between conductances of 0 and 400–600 pS. The pores open and close repeatedly before they finally stabilize at a given conductance, the magnitude of which suggests that it is no larger than twice the 1-nm diam of the gap junction channel (25, 42, 49). The time lag between flow of lipid and aqueous dye depended on the size of the molecule (49). From the lack of movement of aqueous dyes while total fusion pore conductance increased, we surmised that initial HA-triggered fusion events are characterized by the opening of multiple small pores (49).

The order of detectable events during HA-induced fusion with fluorescently labeled RBCs was fusion pore opening, lipid redistribution, and solute redistribution (45, 49). In those studies, this sequence of events was shown only in a few cases since the fibroblasts are very difficult to patch clamp. The extensive data collection on single fusion events reported in this paper (Fig. 3) firmly establish the kinetics of the sequence of events in HA-mediated membrane fusion. Video microscopy observations on single influenza virions fusing with RBC also showed that movement of lipid was restricted during the initial stages of fusion pore opening (22), and that lipid dispersal could occur without redistribution of HA from virus to cell (23). At the early stage, the flow of lipid between the target and viral cell membranes would be severely hindered by the "collar" of protein formed by the transmembrane "anchor" domains of the aggregated HA trimers (see Fig. 6 *A*). The restriction of lipid flow by membrane anchors would explain why the GPI-anchored HA complex, which lacks the transmembrane protein domains, allows free dispersal of lipid in the hemifusion state (20, 26, 49). Movement of the HA trimers away from the complex would break up the collar and allow the flow of lipid between membranes and solute between aqueous compartments.

Monitoring Fusion Pore Opening by Changes in DiI Fluorescence

In this study, we monitored the fusion intermediates of HA-expressing cells with single RBCs labeled with both a fluorescent lipid (DiI) in the membrane and a fluorescent solute (calcein) in the aqueous space, using a fluorescence video microscope that allows for simultaneous, real-time, video rate imaging of up to four fluorophores (34). Fortuitously, in addition to reporting lipid movement during fusion, DiI informed us about the initial formation of the fusion pore by reporting a change in RBC membrane potential ($\Delta\psi$). The fusion pore opening was seen as a decrease in RBC fluorescence, whereas lipid flow was seen as an increase in fibroblast fluorescence (Fig. 2). Tse et al. (45) had originally shown that the decrease in DiI fluorescence occurred concommitantly with fusion pore opening as measured by electrical admittance measurements. The decreases in DiI fluorescence are presumably due to a hyperpolarization of the RBC membrane, which occurs when the RBC inner space becomes continuous with that of the HA-expressing 3T3 cell. Since the RBC membrane is originally at an inside positive membrane potential (18) and the NIH3T3 is negative inside (43), continuity between the two cells will hyperpolarize the RBC membrane. From current transients that represent the discharge of the RBC membrane potential, Spruce et al. (43) deduced $\Delta\psi$s'(fibroblast minus RBC) of ~ -100 mV at the first instance of fusion pore opening. In the case of another commonly used membrane probe, octadecylrhodamine, Leenhouts and De Kruijff (21) had shown that $\Delta\psi$ could be measured as a decrease in fluorescence as a result of hyperpolarization. Recently, Melikyan (Melikyan, G.B., unpublished observations) has obtained similar results with DiI.

As a control for our $\Delta\psi$ measurements using DiI, we monitored cells expressing GPI-anchored influenza virus hemagglutinin that under fusogenic conditions mediate redistribution of fluorescent lipid from RBC membranes to cells without transfer of aqueous dye (hemifusion) (20). By simultaneous video fluorescence microscopy and time-resolved electrical admittance measurements, Melikyan et

Published October 1, 1996

al. (26) rigorously demonstrated that low pH interactions of GPI–HA-expressing cells with planar bilayer membranes resulted in lipid continuity without formation of fusion pores. Since we did not see a decrease in DiI fluorescence with these GPI–HA-expressing cells under fusogenic conditions, but did observe DiI redistribution (Table I), we are confident that the decrease in DiI fluorescence with the wild-type HA-expressing cells indeed informed us about the fusion pore opening.

Kinetics of Stages of Fusion Pore Opening

The onset of fusion of labeled RBC with HA-expressing cells is marked by a change in fluorescence of lipid and/or aqueous dyes. Spectrofluorometric measurements from a population of cells show lag times of 25–100 s between ΔpH and the onset of fluorescence dequenching of membrane and aqueous dyes (9, 31, 38). Since fluorescence dequenching curves from cell populations are convolutions of the individual lag times and redistribution rates (7), it is not possible to obtain information about kinetics of fusion pore opening from those data. In experiments of single cell fusion events, the lag time and rate of dye movement can be measured directly, and therefore kinetics of the processes that allow continuity of membrane and cytoplasmic compartments can be analyzed.

We have attempted to model the kinetics of transition from ΔpH to initial fusion events in terms of aggregation of HA trimers to form a fusion pore (2). This analysis is incomplete, since it does not consider several major factors that may account for the relatively wide range of variations of the characterisitic delay times starting from ΔpH (Fig. 3). They include the geometry of the system, the viscous dissipation of energy in the medium surrounding the membranes or/and in the membranes, and the forces that drive these processes (11). In our laboratory, the delay times have shown to depend on pH (9), temperature (36,40), packing of the target membrane (9,15), and nonadsorbing polymers (16). Although cumulative sums of lag times from ΔpH to initial fusion events have been presented previously (19, 24, 42), the breakthrough in this study is the measurement of the kinetics of transition between two states: from fusion pore to solute permissive fusion pore. The complexity of the intermediary steps from ΔpH to inital fusion events is reflected in the steeper temperature dependence for the ΔpH $\rightarrow$ $\Delta\phi_L$ transition than for the $\Delta\phi_L \rightarrow \Delta\phi_S$ transition (Fig. 5). ΔpH $\rightarrow$ $\Delta\phi_L$ comprises a cascade of stages, most of which involve changes in membrane curvature (8, 35, 41), whereas $\Delta\phi_L \rightarrow \Delta\phi_S$ only involves fusion pore dilation.

Implications for the Design of the Fusion Pore

One of the key questions in the field is how many HA trimers does it take to form a fusion pore. Previously, we had attempted to derive this number from an analysis of aggregation of HA trimers based on measurements of time lags as a function of HA surface density (9). Based on similar data, Danieli et al. (10) recently concluded that a minimum of three, and most likely four, HA trimers is required to initiate the fusion reaction. However, the use of such data for the analysis is incorrect for two principle reasons:

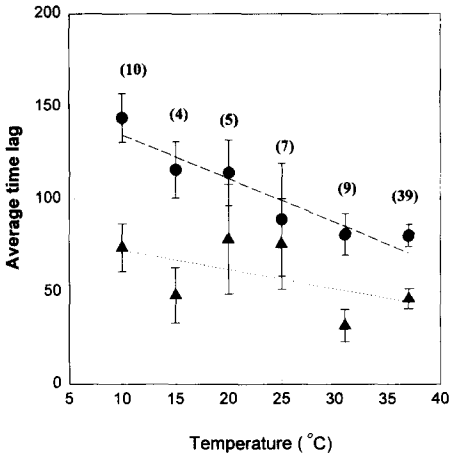

Figure 5. Temperature dependence of HA-mediated fusion events. ●, average time lag for the ΔpH $\rightarrow$ $\Delta\phi_L$ transition. (*Dashed line*) Linear regression through the data points, yielding a slope of −2.35; ▲, average time lag for the $\Delta\phi_L \rightarrow \Delta\phi_S$ transition. (*Dashed line*) Linear regression yielding a slope of −1.04. The numbers in brackets denote the number of observations at each temperature.

(*a*) the time lags were taken from spectrofluorometric measurements (populations of cells) and are convoluted with redistribution rates; (*b*) in addition to aggregation of HA trimers, there is a plethora of other processes within the time lag between ΔpH and lipid mixing. Moreover, the conclusion that a minimum of three, and most likely four, HA trimers is required to initiate the fusion reaction hinges on the misuse of the Hill plot, which is used to analyze equilibrium binding of ligands to proteins. The use of the Hill plot is inappropriate for analyzing kinetics of assembly of the subunits. A log–log plot of the delay time vs concentration of trimers, which is the correct way to analyze these data (2), shows a slope of 1.1 in Fig. 5 (see reference 10). The lack of a higher order slope means that either aggregation is not rate limiting, and/or the fusion pore assembly process is not that simple.

In our analysis, we start with the fusion pore, which already has been formed, and estimate how many subunits need to move to initiate fusion (i.e., movement of large molecules). This way of thinking is similar to that proposed for ion channels by Hodgkin and Huxley (17), who estimated how many subunits need to move in an existing pore to enable flow of ions. We model events that occur as a result of transitions between a FP and a FP_S in the following way: suppose that the fusion pore consists of n HA trimers, each of which can be in one of two states, A and B (Fig. 6). We define p as the probability that a given trimer is in state B. The rate of transition from A to B is given by:

$$dp/dt = \alpha(1 - p) - \beta_l \quad (1)$$

where α and β are forward and backward rate constants, respectively. Eq. 1 has the solution:

$$p = p_\infty(1 - e^{-kt}) \quad (2)$$

where $k = \alpha + \beta$, and $p_\infty = \alpha/(\alpha + \beta)$. If FP_S events will only occur if all n trimers are in state B, the probability p_S of a fusion-permissive fusion pore is given by $p_S = p^n$. The

Published October 1, 1996

number of events yielding a solute-permissive fusion pore is then given by $FP_S = FP_T p^n$, where FP_T is the total number of fusion pores. Therefore the rate of transition to the solute-permissive fusion pore is given by:

$$y = y_\infty (1 - e^{-kt})^n \quad (3)$$

where y and y_∞ are the number of solute-permissive fusion pores at time t and at the steady state, respectively. Curve fitting our data to Eq. 3 using Tablecurve™ (Jandel Scientific) produced $n = 6.3 \pm 0.5$. In Fig. 4, we have drawn the lines according to Eq. 3 with $n = 5$, $n = 6$, and $n = 7$. The $n = 5$ curve shows only one data point to the left of the line, and the $n = 7$ shows a few data points to the right of the line, whereas the $n = 6$ curve shows the data points evenly spread to the left and right of the line. We are therefore quite confident that $n = 6$ is a good fit. Since we are only looking at a transition between two states, our conclusion does not require complicated modeling.

The transition from FP to FP_S is not very efficient. It appears to be aborted in ~40% of low pH–induced fusion events involving labeled erythrocytes bound to HA-express-

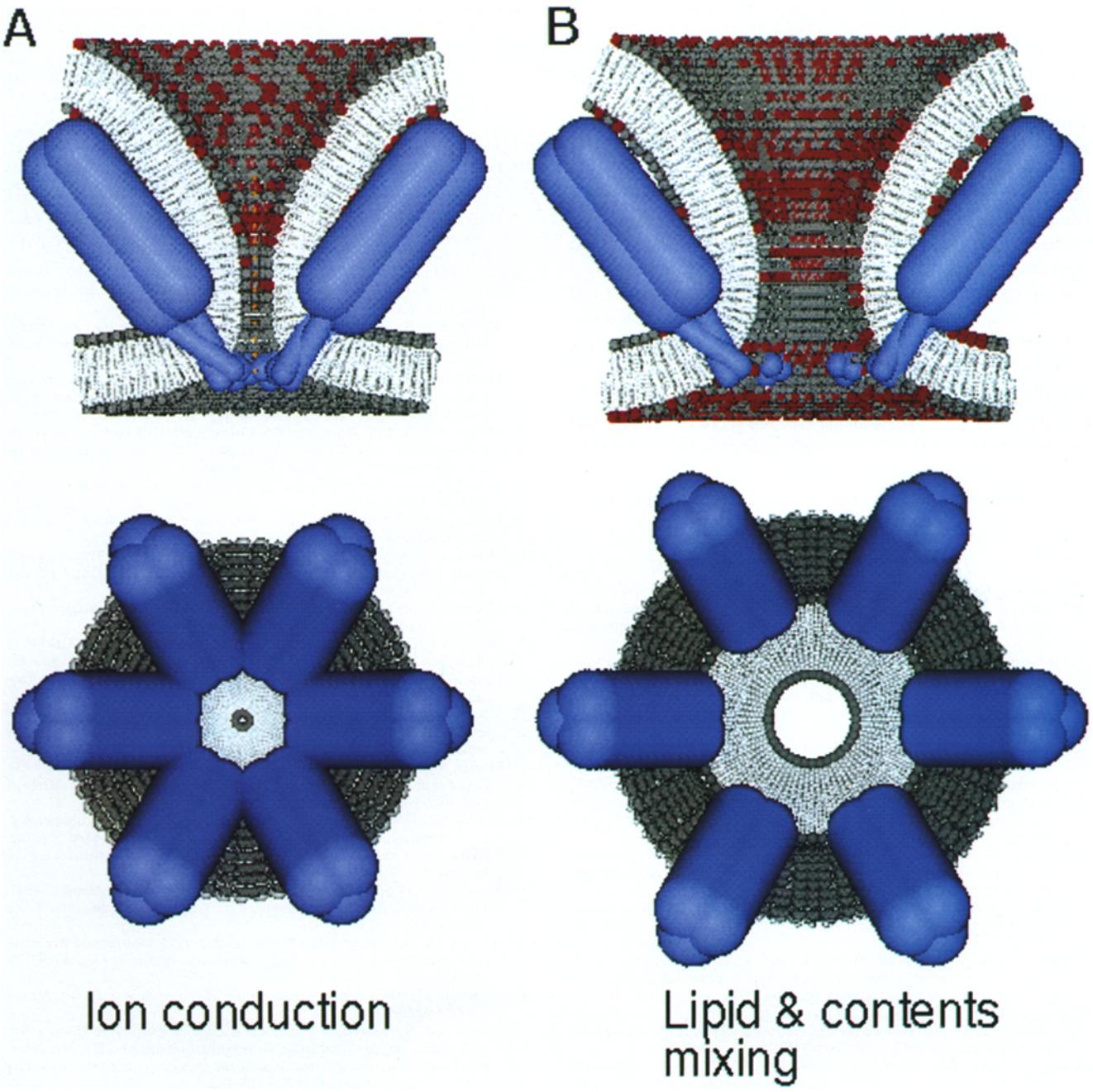

Figure 6. Proposed model for the FP to FP_S transition. The HA protein is represented by blue cylinders, the lipid alkyl chains are in light gray, the lipid headgroups are in dark gray, and the headgroups of the fluorescent DiI label are in red. (*Top*) View perpendicular to the plane of the membrane; (*bottom*) view onto the plane of the membrane. (*A*) Initial pore formation (FP); lipid mixing is prevented by protein collar of transmembrane domains. (*B*) Solute-permissive fusion pore (FP_S).

ing cells (39, 42). Interestingly, single site mutations in the fusion peptide did not affect lipid flow but significantly impaired the ability of HA to mediate delivery of large aqueous molecules from RBC to HA-expressing cells (39). Since the solute-permissive fusion pore requires six HA trimers to be in the right place, our model provides an explanation for these data.

Membrane fusion is ubiquitous in biological systems, occurring in the simplest of unicellular eukaryotes as well as in higher eukaryotes. It provides a mechanism for the regulation of intracellular traffic between different membrane-bound compartments. In the case of exocytosis, Fernandez and co-workers (27, 28) have proposed that a macromolecular scaffold of proteins is responsible for bringing the plasma membrane close to the secretory granule membranes and creating the architecture that enables lipid bilayers to merge (27–29). Evidence is now accumulating that there are several highly conserved families of proteins associated with vesicle fusion events, from yeast to mammalian cells, as well as for intracellular traffic, regulated exocytosis, and synaptic transmission (14, 37, 44). The molecular structures (or scaffolds) that regulate membrane fusion are likely to contain related proteins and to share certain fundamental properties. We had proposed that an assembly of viral envelope glycoproteins could form such a molecular scaffold (1, 3, 4). Our detailed description of pore dilation with the relatively simple HA model system might provide a better understanding of such processes in cell biological systems.

We thank Dr. Judith M. White for her generous gift of the cell lines, and Drs. Anu Puri, Peter Hug, Philip Jones, Thomas Korte, and Dimiter Dimitrov for their help and insightful comments.

Received for publication 20 May 1996 and in revised form 13 July 1996.

References

1. Blumenthal, R. 1988. Cooperativity in viral fusion. *Cell. Biophys.* 12:1–12.
2. Blumenthal, R., C. Schoch, A. Puri, and M.J. Claque. 1991. A dissection of steps leading to viral envelope protein-mediated membrane fusion. *Ann. NY Acad. Sci.* 635:285–296.
3. Blumenthal, R., C.C. Pak, M. Krumbiegel, R.J. Lowy, A. Puri, H.F. Elson, and D.S. Dimitrov. 1994. How viral envelope glycoproteins negotiate the entry of genetic material into the cell. *In* Biotechnology Today. R. Verna and A. Shamoo, editors. Ares-Serono Symposia Publications, Rome, Italy. 151–173.
4. Blumenthal, R., C.C. Pak, Y. Raviv, M. Krumbiegel, L.D. Bergelson, S.J. Morris, and R.J. Lowy. 1995. Transient domains induced by influenza haemagglutinin during membrane fusion. *Mol. Membr. Biol.* 12:135–142.
5. Breckenridge, L.J., and W. Almers. 1987. Currents through the fusion pore that forms during exocytosis of a secretory vesicle. *Nature (Lond.).* 328: 814–817.
6. Chandler, D.E., and J. Heuser. 1979. Membrane fusion during secretion: cortical granule exocytosis in sex urchin eggs as studied by quick-freezing and freeze-fracture. *J. Cell Biol.* 83:91–108.
7. Chen, Y., and R. Blumenthal. 1989. On the use of self-quenching fluorophores in the study of membrane fusion kinetics. *Biophys. Chem.* 34: 283–292.
8. Chernomordik, L.V., G.B. Melikyan, and Y.A. Chizmadzhev. 1987. Biomembrane fusion: a new concept derived from model studies using two interacting planar lipid bilayers. *Biochim. Biophys. Acta.* 906:309–352.
9. Clague, M.J., C. Schoch, and R. Blumenthal. 1991. Delay time for influenza virus hemagglutinin-induced membrane fusion depends on hemagglutinin surface density. *J. Virol.* 65:2402–2407.
10. Danieli, T., S.L. Pelletier, Y.I. Henis, and J.M. White. 1996. Membrane fusion mediated by the influenza virus hemagglutinin requires the concerted action of at least three hemagglutinin trimers. *J. Cell Biol.* 133: 559–569.
11. Dimitrov, D.S., and R. Blumenthal. 1992. Kinetics of intermembrane interactions leading to fusion. *In* Cell and Model Membrane Interactions. S. Ohki, editor. Plenum Publishing Co., New York. 229–247.
12. Ellens, H., J. Bentz, D. Mason, F. Zhang, and J.M. White. 1990. Fusion of influenza hemagglutinin-expressing fibroblasts with glycophorin-bearing liposomes: role of hemagglutinin surface density. *Biochemistry.* 29:9697–9707.
13. Fernandez, J.M., E. Neher, and B.D. Gomperts. 1984. Capacitance measurements reveal stepwise fusion events in degranulating mast cells. *Nature (Lond.).* 312:453–455.
14. Ferro-Novick, S., and R. Jahn. 1994. Vesicle fusion from yeast to man. *Nature (Lond.).* 370:191–193.
15. Herrmann, A., M.J. Clague, and R. Blumenthal. 1993. The role of the target membrane structure in fusion with influenza virus: effect of modulating erythrocyte transbilayer phospholipid structure. *Membr. Biochem.* 10:3–15.
16. Herrmann, A., M.J. Clague, and R. Blumenthal. 1993. Enhancement of viral fusion by nonadsorbing polymers. *Biophys. J.* 65:528–534.
17. Hodgkin, A.L., and A.F. Huxley. 1951. A quantitative description of membrane currents and its application to conduction and excitation in nerve. *J. Physiol.* 117:500–544.
18. Hoffmann, J.F., and P.C. Laris. 1974. Determination of membrane potentials in human and amphiuma red blood cells by means of a fluorescence probe. *J. Physiol.* 239:519–552.
19. Kaplan, D., J. Zimmerberg, A. Puri, D.P. Sarkar, and R. Blumenthal. 1991. Single cell fusion events induced by influenza hemagglutinin: studies with rapid-flow, quantitative fluorescence microscopy. *Exp. Cell. Res.* 195: 137–144.
20. Kemble, G.W., T. Danieli, and J.M. White. 1994. Lipid-anchored influenza hemagglutinin promotes hemifusion, not complete fusion. *Cell.* 76:383–391.
21. Leenhouts, J.M., and B. De Kruijff. 1995. Membrane potential-driven translocation of a lipid-conjugated rhodamine. *Biochim. Biophys. Acta.* 1237:121–126.
22. Lowy, R.J., D.P. Sarkar, Y. Chen, and R. Blumenthal. 1990. Single influenza virus-cell fusion events observed by fluorescenct video microscopy. *Proc. Natl. Acad. Sci. USA.* 87:1850–1854.
23. Lowy, R.J., D.P. Sarkar, M.H. Whitnall, and R. Blumenthal. 1995. Differences in dispersion of influenza virus lipids and proteins during fusion. *Exp. Cell. Res.* 216:411–421.
24. Melikyan, G.B., W.D. Niles, and F.S. Cohen. 1993. Influenza virus hemagglutinin-induced cell-planar bilayer fusion: quantitative dissection of fusion pore kinetics into stages. *J. Gen. Physiol.* 102:1151–1170.
25. Melikyan, G.B., W.D. Niles, M.E. Peeples, and F.S. Cohen. 1993. Influenza hemagglutinin-mediated fusion pores connecting cells to planar membranes: flickering to final expansion. *J. Gen. Physiol.* 102:1131–1149.
26. Melikyan, G.B., J.M. White, and F.S. Cohen. 1995. GPI-anchored influenza hemagglutinin induces hemifusion to both red blood cell and planar bilayer membranes. *J. Cell. Biol.* 131:679–691.
27. Monck, J.R., and J.M. Fernandez. 1992. The exocytotic fusion pore. *J. Cell. Biol.* 119:1395–1404.
28. Monck, J.R., and J.M. Fernandez. 1994. The exocytotic fusion pore and neurotransmitter release. *Neuron.* 12:707–716.
29. Monck, J.R., A.F. Oberhauser, and J.M. Fernandez. 1995. The exocytotic fusion pore interface: a model of the site of neurotransmitter release. *Mol. Membr. Biol.* 12:151–156.
30. Morris, S.J. 1990. Real-time multi-wavelength fluorescence imaging of living cells. *Biotechniques.* 8:296–308.
31. Morris, S.J., D.P. Sarkar, J.M. White, and R. Blumenthal. 1989. Kinetics of pH-dependent fusion between 3T3 fibroblasts expressing influenza hemagglutinin and red blood cells. Measurement by dequenching of fluorescence. *J. Biol. Chem.* 264:3972–3978.
32. Morris, S.J., J. Zimmerberg, D.P. Sarkar, and R. Blumenthal. 1993. Kinetics of cell fusion mediated by viral spike glycoproteins. *Methods Enzymol.* 221:42–58.
33. Morris, S.J., T.B. Wiegmann, L.W. Welling, and B.M. Chronwall. 1994. Rapid simultaneous estimation of intracellular calcium and pH. *Methods Cell. Biol.* 40:183–220.
34. Morris, S.J., D.E. Howard, T.H. Chang, D.P. Sarkar, and R. Blumenthal. 1995. Hemagglutinin-catalyzed cell-cell fusion: kinetics of initial pore formation from video rate, multi-wavelength fluorescence microscopy. *J. Microsc. Soc. Am.* 1:47–54.
35. Nanavati, C., V.S. Markin, A.F. Oberhauser, and J.M. Fernandez. 1992. The exocytotic fusion pore modeled as a lipidic pore. *Biophys. J.* 63: 1118–1132.
36. Pak, C.C., M. Krumbiegel, and R. Blumenthal. 1994. Intermediates in influenza PR/8 hemagglutinin-induced membrane fusion. *J. Gen. Virol.* 75: 395–399.
37. Rothman, J.E. 1994. Mechanisms of intracellular protein transport. *Nature (Lond.).* 372:55–63.
38. Sarkar, D.P., S.J. Morris, O. Eidelman, J. Zimmerberg, and R. Blumenthal. 1989. Initial stages of influenza hemagglutinin-induced cell fusion monitored simultaneously by two fluorescent events: cytoplasmic continuity and lipid mixing. *J. Cell. Biol.* 109:113–122.
39. Schoch, C., and R. Blumenthal. 1993. Role of the fusion peptide sequence in initial stages of influenza hemagglutinin-induced cell fusion. *J. Biol. Chem.* 268:9267–9274.
40. Schoch, C., R. Blumenthal, and M.J. Clague. 1992. A long-lived state for influenza virus-erythrocyte complexes committed to fusion at neutral pH. *FEBS Lett.* 311:221–225.

41. Siegel, D.P. 1993. Energetics of intermediates in membrane fusion: comparison of stalk and inverted micellar intermediate mechanisms. *Biophys. J.* 65:2124–2140.
42. Spruce, A.E., A. Iwata, J.M. White, and W. Almers. 1989. Patch clamp studies of single cell-fusion events mediated by a viral fusion protein. *Nature (Lond.).* 342:555–558.
43. Spruce, A.E., A. Iwata, and W. Almers. 1991. The first milliseconds of the pore formed by a fusogenic viral envelope protein during membrane fusion. *Proc. Natl. Acad. Sci. USA.* 88:3623–3627.
44. Sudhof, T.C. 1995. The synaptic vesicle cycle: a cascade of protein-protein interactions. *Nature (Lond.).* 375:645–653.
45. Tse, F.W., A. Iwata, and W. Almers. 1993. Membrane flux through the pore formed by a fusogenic viral envelope protein during cell fusion. *J. Cell. Biol.* 121:543–552.
46. White, J., K. Matlin, and A. Helenius. 1981. Cell fusion by Semliki forest, influenza, and vesicular stomatitis viruses. *J. Cell Biol.* 89:674–679.
47. Wilson, I.A., J.J. Skehel, and D.C. Wiley. 1981. Structure of the haemagglutinin membrane glycoprotein of influenza virus at 3 A resolution. *Nature (Lond.).* 289:366–373.
48. Zimmerberg, J., M. Curran, F.S. Cohen, and M. Brodwick. 1987. Simultaneous electrical and optical measurements show that membrane fusion precedes secretory granule swelling during exocytosis of beige mouse mast cells. *Proc. Natl. Acad. Sci. USA.* 84:1585–1589.
49. Zimmerberg, J., R. Blumenthal, D.P. Sarkar, M. Curran, and S.J. Morris. 1994. Restricted movement of lipid and aqueous dyes through pores formed by influenza hemagglutinin during cell fusion. *J. Cell. Biol.* 127: 1885–1894.